Packaging of a Flexible Polyelectrolyte Inside a Viral Capsid: Effect of Salt Concentration and Salt Valence†

Daniel George Angelescu,‡ Joakim Stenhammar, and Per Linse*

Physical Chemistry 1, Lund University, P.O. Box 124, SE-221 00 Lund, Sweden

Received: December 6, 2006; In Final Form: May 19, 2007

The effect of salt on the location and structure of a flexible polyelectrolyte confined inside a viral capsid and the Donnan equilibrium of the salt across the capsid have been examined using a coarse-grained model solved by Monte Carlo simulations. The polyelectrolyte was represented by a linear jointed chain of charged beads, and the capsid was represented by a spherical shell with embedded charges. At low salt concentration, the polyelectrolyte was strongly adsorbed onto the inner capsid surface, whereas at high salt concentration it was located preferentially in the central part of the capsid. Under the condition of equal Debye screening length, the electrostatic screening increased as the valence of the polyelectrolyte counterion was increased. The distribution of the small cations and anions was unequal across the capsid. An excess of polyelectrolyte counterions occurred inside the capsid, and the excess increased with the salt concentration. A simplified representation of the small ions through the use of the screened Coulomb potential provided only a qualitatively correct picture; the electrostatic screening originating from the small ions was exaggerated.

Introduction

A viral particle is an exceptional example of macromolecular self-assembly in nature.[1] It consists in essence of a charged protein shell (capsid) that encloses the oppositely charged genetic material (RNA or DNA). A number of experiments illustrate that the self-assembly of viruses can be performed in vitro from purified DNA and RNA and the basic components of the capsid under the right ionic strength and pH.[2−4] The capsid self-assembly is driven by the hydrophobic interaction between capsid proteins. Additionally, it is believed that electrostatics, in particular the electrostatic attraction between the capsid and the genome, is important for the self-assembly of RNA-containing viruses.[5]

On the basis of experiments concerning the location of ssRNA viral genome inside the capsid, it was concluded that a tight association of a significant part of the genome with the capsid occurred[6] and that the density of that part of the genome is similar to that encountered in RNA crystals.[7] Viral dsDNA is also packaged into the capsid to near-crystalline density,[8] and it exhibits long-range ordering.[9] The most frequent structure of packaged dsDNA is the so-called coaxial spool.[10−12] This organization arises simply from the bending resistance of the genome in the encapsidation process, and the electrostatic attraction between the genome and the capsid is thus less important in stabilizing the spool. Nonetheless, the presence of polyvalent cations or other condensing agents inside the capsid can trigger a local hexagonal coordination in the spool, and the corresponding ds spacing is related to the presence of the counterions that fills the region between adjacent DNA strands.[9] The presence of condensing agents such as spermine and spermidine was also found inside RNA viruses,[13,14] and their presence is believed to be instrumental in terms of RNA packaging, even though their function is not well-understood. It has been also shown that the ejection force of DNA from phages can in vitro be significantly reduced by addition of di- and polyvalent salts.[15,16] However, the conditions in solutions commonly used for in vitro phage experiments include a buffering agent such as tris(hydroxymethyl)aminomethane (Tris), which adds monovalent ions to the original di- or polyvalent salt.

Because of the size and complexity of viruses, computer simulations of fully atomistic models are yet hardly feasible, and consequently, most of the virus simulation studies used a coarse-grained representation of both the capsid and the viral genome.[10,17−23] For example, the capsid was treated as either an uncharged spherical[17,19,20] or icosahedral shell,[21] whereas the intramolecular interaction of dsDNA under physiological condition was mainly modeled by means of the Lennard−Jones potential.[10,20,21] In spite of their simplifications, coarse-grained models provide an important understanding of generic features of viral packing and assembly. To our best knowledge, the first all-atom molecular dynamics simulation of a complete virus was recently reported by Freddolino et al.[24] The radial distribution of the genome inside a capsid obtained from the all-atom molecular dynamics simulation[24] was astonishingly similar to that predicted by a model where the genome was represented by a chain of connected charged hard spheres, and the capsid was represented by a spherical shell with embedded charges.[22] In addition, many simulation studies involving quite simplistic representations of both the capsid and the encapsidated genome predicted that the dsDNA was arranged in a coaxial spool as observed from electron microscopy studies.[25,26] Furthermore, by using an all-atom model for the capsid and a coarse-grained one for the genome,[27] the crystallographic radial distribution of the genome of ssRNA viruses[7] could be recovered. Finally, recent studies on polyelectrolyte chains and its counterions inside an uncharged capsid-like shell revealed a polyelectrolyte coun-

† Part of the special issue "International Symposium on Polyelectrolytes (2006)".

* Corresponding author.

‡ Permanent address: Romanian Academy, Institute of Physical Chemistry "I. G. Murgulescu", Splaiul Independentei 202, 060021 Bucharest, Romania.

10.1021/jp068384o CCC: $37.00
Published on Web 06/30/2007

terion leakage from the shell interior at low ionic strength that resulted in a polyelectrolyte adsorption onto the inner shell surface.[22,28]

The aim of this work is to address the effect of salt addition and salt valence on (i) the structural properties of a flexible polyelectrolyte representing ssRNA confined inside an oppositely charged spherical shell and (ii) the distribution and environment of the salt species through excess chemical potential calculations. Monte Carlo simulations are performed using the same coarse-grained model with explicit representation of all charged species previously employed when studying the structural properties of encapsidated polyelectrolyte and the free energy associated with the encapsidation process in the salt-free limit.[22,23] In addition, we have assessed the usefulness of a screened Coulomb potential model with an implicit description of the small ions to describe virus systems. The polyelectrolyte was found strongly adsorbed onto the inner capsid surface at low and moderate salt content irrespective of the valence of the polyelectrolyte counterions. As the salt concentration was increased further, a smooth transition from the above-mentioned configuration to a chain uniformly distributed in the central part of the capsid appeared. Moreover, (i) the net charge of the capsid increased with the salt concentration and the polyelectrolyte counterion valence, and (ii) the presence of the charged polyelectrolyte encapsidated in an oppositely charged shell had an important effect on the excess chemical potential of the polyelectrolyte and capsid counterions *inside* the capsid.

Model and Methods

Model. We have used a virus model previously employed to examine the properties of polyelectrolyte-containing capsids at various conditions.[22] The model represents a scaled-down version of a $T = 3$ virus, and the size reduction enables a systematic simulation study. Briefly, the viral capsid was represented by a spherical shell with an inner radius $R_c = 50$ Å and a thickness $D_c = 12$ Å. A discrete and regular capsid charge distribution with the $N_c = 252$ capsid charges positioned at a radial distance $R_c + \Delta$ with $\Delta = 2$ Å was used, leading to a charge density at the inner capsid surface in reasonable agreement with experimental data.[5] These charges were kept permanent; hence, we neglected that the ionic amino acids are weak protolytes, whose charge status depend on the local electrostatic potential. The electrostatic potential inside the capsid originating from the capsid charges is nearly constant; a significant variation ($\approx$1 kT/e) occurs only close to the inner capsid surface.

The polyelectrolyte was modeled as a chain of negatively charged hard spheres (referred to as beads) connected by harmonic bonds. Throughout, we used $N_b = 252$ beads, which corresponds to a charge-neutral polyelectrolyte−capsid complex. The polyelectrolyte was confined inside the capsid, whereas the small ions were allowed to pass through the capsid. The solvent and the capsid were considered as dielectric continua entering the model by the same relative permittivity.

The structure of the polyelectrolyte−capsid complex at different concentrations of simple salt was examined using two different models: (i) the primitive model, where the small ions are treated as charged hard spheres, and (ii) the simplified screened Coulomb model, which does not explicitly include the small ions. In the former case, the cation (polyelectrolyte counterion) valence was $Z_+ = +1$, $+2$, or $+3$, and the anion (capsid counterion) valence was $Z_- = -1$. The corresponding salt solutions are referred to as 1:1, 2:1, and 3:1 solutions, respectively. In the latter model, the influence of the small ions was pre-averaged by using a screened Coulomb potential for the bead−bead and the bead-capsid charge interactions.

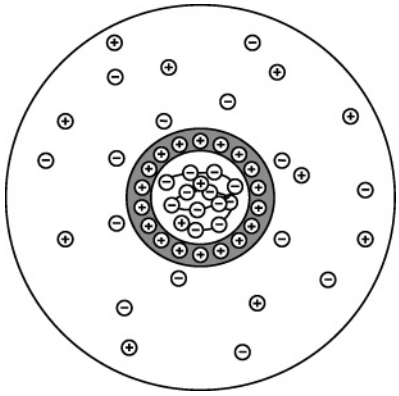

Figure 1. Schematic illustration of a solution containing a polyelectrolyte-containing capsid and simple salt in a spherical cell. The shaded area with embedded charges denotes the capsid. Note, objects are not depicted to scale.

TABLE 1: Data of the Polyelectrolyte-Containing Capsid Model

Cell	
cell radius	$R_{cell} = 100$ Å
temperature	$T = 298$ K
relative dielectric permittivity	$\epsilon_r = 78.4$
Capsid	
inner capsid radius	$R_c = 50$ Å
capsid thickness	$D_c = 12$ Å
no. of capsid charges	$N_c = 252$
capsid charge	$Z_c = +1$
Polyelectrolyte	
no. of beads	$N_b = 252$
bead charge	$Z_b = -1$
bead radius	$R_b = 2$ Å
bead−bead separation	$\langle R_{bb}^2 \rangle^{1/2} \approx 5.7$ Å
bare persistence length	$l_p^0 = 8.5$ Å
Small ions	
small ion radii	$R_+ = R_- = 2$ Å
polyelectrolyte counterion valence	$Z_+ = +1, +2, +3$
capsid counterion valence	$Z_- = -1$

Throughout, the spherical cell approach was used, here implying that the polyelectrolyte-containing capsid and appropriate amount of simple salt forming an electroneutral system are enclosed in a spherical cell, see Figure 1. Values of the parameters characterizing the model are summarized in Table 1.

The total potential energy U is a sum of four contributions according to

$$U = U_{nonbond} + U_{bond} + U_{angle} + U_{cell} \quad (1)$$

The nonbonding term $U_{nonbond}$ is furthermore divided into two contributions

$$U_{nonbond} = \sum_{i<j} u_{ij}(r_{ij}) + \sum_i u_{c,i}(r_{c,i}) \quad (2)$$

where the first term represents interactions among the mobile particles (beads and small ions) and the second one represents the interaction of mobile species with capsid charges. In the case of the primitive model, the first contribution in eq 2 is given by

$$u_{ij}(r_{ij}) = \begin{cases} \infty, & r_{ij} < R_i + R_j \\ \dfrac{Z_i Z_j e^2}{4\pi\epsilon_0\epsilon_r r_{ij}}, & r_{ij} \geq R_i + R_j \end{cases} \quad (3)$$

where i and j denote a mobile particle, R_i is the hard-sphere radius of particle i, Z_i is the valence of particle i, r_{ij} is the distance between the centers of the particles i and j, ϵ_0 is the dielectric permittivity of the vacuum, and ϵ_r is the relative permittivity of the system. The second term in eq 2 can be written as

$$u_{c,i}(r_i) = \begin{cases} \infty, & R_c - R_i < r_i < R_c + D_c + R_i \\ \displaystyle\sum_{j=1}^{N_c} \frac{Z_i Z_j e^2}{4\pi\epsilon_0\epsilon_r r_{ij}}, & \text{otherwise} \end{cases} \quad (4)$$

where r_{ij} denotes the distance between the mobile particle i and the capsid charge j and N_c denotes the number of capsid charges.

Within the screened Coulomb model, the summation in eq 2 extends only over beads, and $u_{ij}(r_{ij})$ and $u_{c,i}(r_j)$ are given by the following extended Debye−Hückel potentials

$$u_{ij}(r_{ij}) = \begin{cases} \infty, & r_{ij} < R_i + R_j \\ \dfrac{Z_i Z_j e^2}{4\pi\epsilon_0\epsilon_r r_{ij}} \dfrac{\exp[-\kappa(r_{ij} - (R_i + R_j))]}{(1 + \kappa R_i)(1 + \kappa R_j)}, & r_{ij} \geq R_i + R_j \end{cases} \quad (5)$$

$$u_{c,i}(r_i) = \begin{cases} \infty, & R_c - R_i < r_i < R_c + D_c + R_i \\ \displaystyle\sum_{j=1}^{N_c} \frac{Z_i Z_j e^2}{4\pi\epsilon_0\epsilon_r r_{ij}} \frac{\exp[-\kappa(r_{ij} - R_i)]}{(1 + \kappa R_i)}, & \text{otherwise} \end{cases} \quad (6)$$

The Debye screening length κ^{-1} entering in eqs 5 and 6 is given by

$$\kappa^2 = \frac{e^2}{\epsilon_0\epsilon_r kT} \sum_l z_l^2 \rho_l \quad (7)$$

where l refers to the small ions, ρ_l is the number density of the small ion of type l, k is the Boltzmann constant, and T is the absolute temperature.

The second term of eq 1, the bond energy U_{bond}, is represented by

$$U_{bond} = \sum_{i=1}^{N_b - 1} \frac{k_{bond}}{2} (r_{i,i+1} - r_0)^2 \quad (8)$$

where $r_{i,i+1}$ is the distance between two adjacent beads in the chain, r_0 is the equilibrium bond distance ($r_0 = 5$ Å), and k_{bond} is the bond force constant ($k_{bond} = 0.4$ N m^{-1}).

The angular potential energy U_{angle} in eq 1 is given by

$$U_{angle} = \sum_{i=2}^{N_b - 1} \frac{k_{angle}}{2} (\alpha_i - \alpha_0)^2 \quad (9)$$

where α_i is the angle between the bond vectors $\mathbf{r}_{i+1} - \mathbf{r}_i$ and $\mathbf{r}_{i-1} - \mathbf{r}_i$ made by three consecutive beads, α_0 is the equilibrium angle ($\alpha_0 = 180°$), and k_{angle} is the angular force constant. In this study, $k_{angle} = 0.51 \times 10^{-24}$ J deg^{-2}, and the bare persistence length, evaluated for the corresponding uncharged chain, is $l_p^0 = 8.5$ Å.[29] This bare persistence length is considered to model a homopolymeric *ss*RNA.

TABLE 2: Number of Polyelectrolyte Counterions N_+ and Capsid Counterions N_- and the Debye Screening Length κ^{-1} of the Different Salt Solutions

N_+	N_-	κ^{-1} (Å)
	$Z_+ = +1, Z_- = -1$	
8	8	54.0
51	51	21.4
252	252	9.61
574	574	6.37
1293	1293	4.25
5174	5174	2.12
	$Z_+ = +2, Z_- = -1$	
2	4	62.3
17	34	21.4
77	154	10.6
126	252	7.85
191	382	6.38
431	862	4.25
1724	3448	2.12
	$Z_+ = +3, Z_- = -1$	
2	6	44.1
8	24	22.0
39	117	9.98
84	252	7.00
215	645	4.25
862	2586	2.12

The term U_{cell} in eq 1 describes the confining cell potential, and it is given by

$$U_{cell} = \sum_i u_{cell}(r_i) \quad (10)$$

with

$$u_{cell}(r_i) = \begin{cases} 0, & r_i < R_{cell} \\ \infty, & r_i \geq R_{cell} \end{cases} \quad (11)$$

To enable simulations at high salt concentrations, a fairly small cell was used, namely, $R_{cell} = 100$ Å. At the highest salt concentration, 2.3 M, approximately 10 300 small ions are present in the system. Table 2 provides an overview of the numbers of polyelectrolyte and capsid counterions and the corresponding Debye screening lengths considered.

Simulation Details. The properties of the model systems were evaluated by performing Metropolis Monte Carlo (MC) simulations in the canonical ensemble. No potential cutoff was applied. The polyelectrolyte beads were subjected to three types of trial displacements: (i) translation of a single bead, (ii) slithering move, and (iii) pivot rotation. The small ions were subjected to single-particle displacements only.

Simulations were started from initial configurations generated by randomly placing the polyelectrolyte beads inside the capsid and by placing the small ions throughout the whole cell using hard-sphere overlap checks and bond constraints. After an equilibration of 2×10^5 passes (attempted moves per particle), production runs of typically 10^6 passes were carried out. The sampling of the excess chemical potential of the ionic species was made in separate production runs involving in total 10^7 trial insertions.

The statistical uncertainties given are one standard deviation of the mean and were calculated by dividing the total simulation into 10 sub-batches. The simulations were performed by using the integrated Monte Carlo/molecular dynamics/Brownian dynamics simulation package MOLSIM.[30]

Structural Analysis and Excess Chemical Potential Evaluation. The radial position of the mobile particles was described by the radial density distribution $\rho(r)$ representing the number density of the particles at the radial distance r. Furthermore, the associated running coordination number $\mathrm{rcn}(r) = \int_0^r 4\pi r'^2 \rho(r')\, dr'$ was used to determine the number of encapsidated small ions.

The radial extension of encapsidated polyelectrolytes was quantified by the radius of gyration R_G given by

$$R_G^2 = \frac{1}{N_b}\sum_{i=1}^{N_b} |\mathbf{r}_i - \mathbf{r}_{com}|^2 \tag{12}$$

where $\mathbf{r}_i$ is the position vector of bead i and $\mathbf{r}_{com}$ is the location of the center of mass of the polyelectrolyte.

The excess chemical potential of the individual small ions μ_i^{ex} was evaluated by applying Widom's insertion method.[31] Since the inserted particle was charged, a charge compensation was achieved by a charge rescaling of the whole system.[32] The excess chemical potential of species i is given by

$$\mu_i^{ex} = -kT \ln\langle \exp(-\Delta U_i^{test}/kT)\rangle \tag{13}$$

where ΔU^{test} is the potential energy difference due to the particle insertion. The excess chemical potential of the small ions was separately evaluated inside and outside the capsid. The excess chemical potential of the simple salt μ^{ex} is related to the excess chemical potential of the individual salt species through

$$\mu^{ex} = \nu_+ \mu_+^{ex} + \nu_- \mu_-^{ex} \tag{14}$$

where ν_- and ν_+ refer to the chemical composition of the salt. For example $\nu_+ = 1$ and $\nu_- = 3$ for the 3:1 salt solution.

The excess chemical potential of the salt species in a pure salt solution was also evaluated. This was performed by using a cubic box with periodical boundary conditions, and the Ewald summation method was applied.[33] Moreover, the corresponding excess chemical potentials were also calculated using a spherical cell. Not unexpected, the different boundary conditions affected the outcome; however, the differences were small in comparison with the effects of the presence of the capsid and polyelectrolyte and will not be discussed further.

Results

In the following, the properties of the polyelectrolyte-containing capsid will be examined on the basis of the results from the primitive model. Thereafter, a comparison of the results obtained from the primitive and screened Coulomb models will be presented.

Primitive Model. In the case of the primitive model, the role of the polyelectrolyte counterion valence at an intermediate salt concentration will first be considered. That will be followed by an account of the dependence of the salt concentration and polyelectrolyte counterion valence on structural properties and the excess chemical potential of the small ions.

Intermediate Salt Concentration. We consider the 1:1, 2:1, and 3:1 salt solutions at the salt concentration $c_{salt}|Z_+| = 113$ mM. This concentration is achieved by introducing cations and anions as counterions that separately neutralize the charge of the polyelectrolyte and the capsid, respectively. The corresponding Debye screening lengths of the three salt solutions become $\kappa^{-1} = 9.6$, 7.9, and 7.0 Å. Figure 2 provides typical snapshots of the interior of the capsid for the three different salt solutions. The polyelectrolyte is locally folded, and the spatial correlations

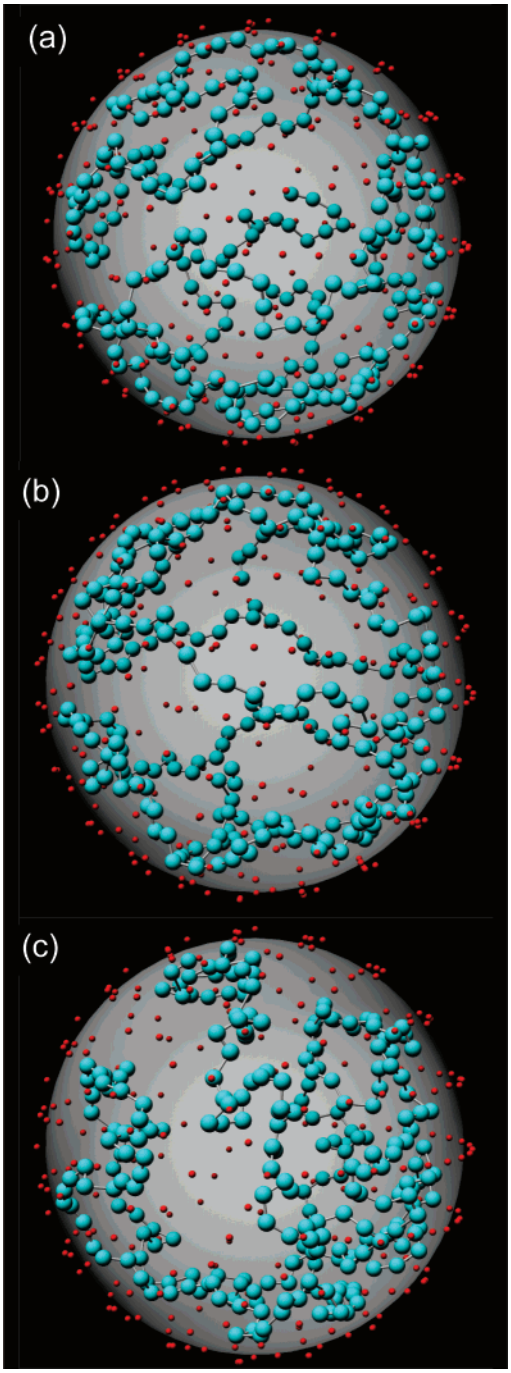

Figure 2. A polyelectrolyte is confined inside a charged spherical capsid that is located in a spherical cell containing (a) 1:1, (b) 2:1, and (c) 3:1 simple salt. The snapshots illustrate typical configurations of the polyelectrolyte beads (blue connected spheres) and the location of the inner capsid surface (gray sphere) and of the capsid charges (red dots). The small ions are omitted for clarity.

along the chain contour are much smaller than the inner capsid radius. Moreover, it appears that the chain is distributed across the whole interior of the capsid.

The bead and small ion number densities as functions of the radial distance with respect to the center of the capsid are displayed in Figure 3. Generally, the beads are located close to the inner capsid surface (Figure 3a), a result similar to that reported for a more diluted system ($R_{cell} = 561.1$ Å) with a larger Debye screening length of ($\kappa^{-1} = 128$ Å).[22] At a closer inspection, as the polyelectrolyte counterion valence Z_+ is increased, (i) the bead density at contact with the inner capsid surface decreases, (ii) the location of the maximum of the bead

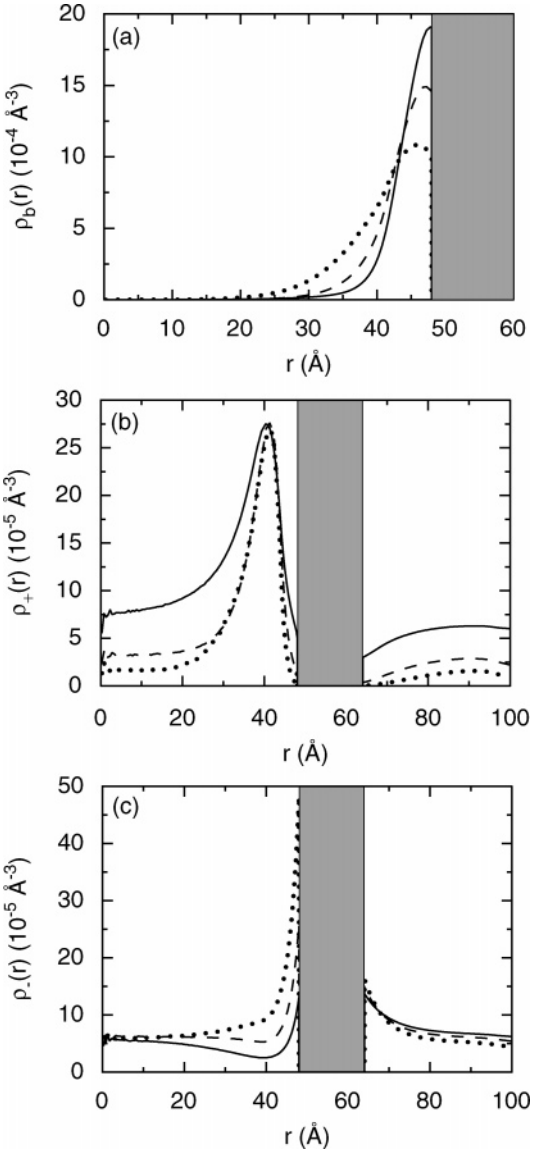

Figure 3. (a) Bead number density $\rho_b(r)$, (b) polyelectrolyte counterion number density $\rho_+(r)$, and (c) capsid counterion number density $\rho_-(r)$ as a function of the radial distance r in 1:1 (solid curves), 2:1 (dashed curves), and 3:1 (dotted curves) salt solution at $c_{salt}|Z_+| = 113$ mM. The shaded areas denote the location of the capsid.

number density is weakly shifted from the capsid surface toward the center of the capsid, and (iii) the extension of the bead-free central region of the capsid is reduced. For example, $\rho(R_c - R_b)$ decreases by ≈40%, and the radius of the central void reduces from 30 Å to 20 Å when the monovalent cations are replaced by trivalent ones.

The radial profiles of the polyelectrolyte counterions $\rho_+(r)$ are at the different cationic valences qualitatively similar (Figure 3b). The concentrations are nearly constant close to the capsid center ($r < 20$ Å), display a maximum near the inner capsid surface ($r \approx 40$ Å), and decrease strongly closer to the inner capsid surface (40 Å $< r <$ 48 Å), the interval where most of the beads reside. The location and the value at the maximum of ρ_+ are independent of Z_+, implying that the cation charge density $Z_+\rho_+$ at the maximum is proportional to Z_+, whereas the cation charge density $Z_+\rho_+$ at the capsid center is nearly independent of Z_+. Outside the capsid ($r > 64$ Å), the cations are depleted, not only from the outer capsid surface but also from the cell boundary. The maximum cation concentration between the two depletion regions is somewhat smaller than that in the center of the capsid for all Z_+.

There is a considerable accumulation of capsid counterions at both capsid surfaces (Figure 3c), despite the polyelectrolyte−capsid charge ratio being unity. The anions are homogeneously distributed in the central volume of the capsid ($r < 20$ Å) as well as in a region outside the capsid ($r > 80$ Å). The number density of the capsid counterions at the two capsid surfaces differs. With monovalent cations, ρ_- is largest on the outside, while the opposite holds for $Z_+ = 2$ and 3. Whereas ρ_- at the outer surface is essentially independent of Z_+, the contact density at the inner surface increases nearly linearly with Z_+ from 12 $\times 10^{-5}$ Å^{-3} for $Z_+ = 1$ to 48 $\times 10^{-5}$ Å^{-3} for $Z_+ = 3$. This increase likely originates from the increase of the charge density of polyelectrolyte counterions at $r \approx 40$ Å. Moreover, the capsid counterion distributions display a weak depletion at about $r \approx 40$ Å for $Z_+ = 1$ and 2, whereas no depletion occurs for $Z_+ = 3$.

The polyelectrolyte counterion valence has an important effect on the number of small ions found inside the capsid and thus on the net charge of the polyelectrolyte-containing capsid. The charge of the polyelectrolyte counterions residing inside the capsid increases from 73.4 ± 0.3e for $Z_+ = 1$ to 143 ± 2e for $Z_+ = 3$, and the corresponding change of the charge of the capsid counterions is −19.3 ± 0.3e and −54.5 ± 0.7e. Hence, the strengthened interaction between polyelectrolyte and its counterions leads to an increase of the capsid net charge Z_c^{net} from 54.1 to 89, corresponding to a 63% increase. Finally, we notice that the capsid counterion distribution contrasts that for a more dilute neutral polyelectrolyte−capsid complex (R_{cell} = 561.1 Å and $\kappa^{-1} = 128$ Å), where nearly no capsid counterions were found inside the capsid.[22]

To conclude, the polyelectrolyte counterion valence affects quantitatively the radial distribution of all charged species and the capsid net charge. An increase of the valence leads to (i) a decrease of the bead density at contact with the inner capsid surface and an extension of the polyelectrolyte toward the capsid center, (ii) a linear increase of the charge density of the polyelectrolyte counterions at $r \approx 40$ Å and of capsid counterion density at contact with the inner capsid surface, and (iii) an increase of the capsid net charge. With monovalent cations, the polyelectrolyte is firmly adsorbed to the inner capsid surface, enabling a release of the capsid counterions from the capsid. As the cation valence is increased, the stronger polyelectrolyte−cation interaction leads to an enhanced accumulation of cations near the polyelectrolyte, which then becomes partly detached from the inner capsid surface, as well as to an increased amount of capsid counterions inside the capsid.

Variation of Salt Concentration. Structural Effects. The effect of the salt concentration on the radial distribution of the mobile particles and the polyelectrolyte conformation will now be examined. The qualitative dependence of the salt concentration on the radial density profiles of each of the mobile particles was found to be similar for the three salt solutions. Therefore, detailed results will only be given for the 3:1 salt solution.

Figure 4 shows the bead number density $\rho_b(r)$ and the reduced number density of small ions $\rho_i(r)/N_i$ as a function of the radial distance r for the 3:1 salt solution at concentrations corresponding to $\kappa^{-1} = 44$, 7.0, and 2.1 Å. Regarding the small ions, the normalized quantity $\rho_i(r)/N_i$ is given to handle the nearly 400-fold variation of the salt concentration. The intermediate salt concentration in the previous subsection corresponded to $\kappa^{-1} = 7.0$ Å.

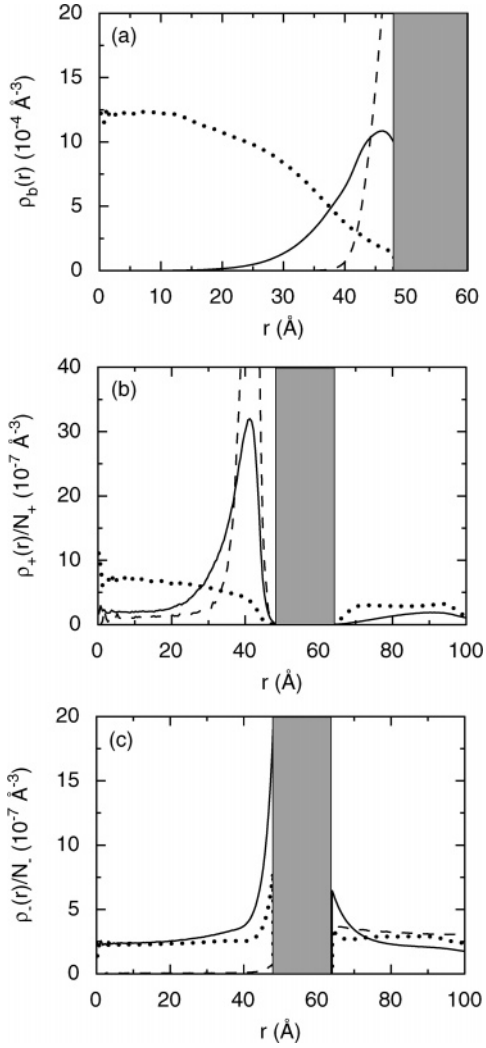

Figure 4. (a) Bead number density $\rho_b(r)$, (b) reduced polyelectrolyte counterion number density $\rho_+(r)/N_+$, and (c) reduced capsid counterion number density $\rho_-(r)/N_-$ as a function of the radial distance r in 3:1 salt solution at salt concentrations corresponding to the Debye screening length $\kappa^{-1} = 44$ Å (dashed curves), $\kappa^{-1} = 7.0$ Å (solid curves), and $\kappa^{-1} = 2.1$ Å (dotted curves). The shaded areas denote the location of the capsid.

As compared with the intermediate salt concentration (solid curve), the accumulation of the beads to the inner capsid surface at $\kappa^{-1} = 44$ Å (dashed curve) becomes much stronger (Figure 4a). At concentrations above the intermediate one, the bead density at the inner capsid surface is considerably reduced, and the concentration of beads close to the capsid center increases. At $\kappa^{-1} = 2.1$ Å (dotted curve), the beads are preferentially accumulated in the central part of the capsid and depleted near the inner capsid surface. The bead profile here is similar to that reported for a weakly charged polymer confined inside a spherical and uncharged cavity.[34]

The polyelectrolyte counterion distribution $\rho_+(r)/N_+$ (Figure 4b) follows closely the changes of the distribution of the beads. Hence, the amplitude of the maximum at $r = 40$ Å is largest at $\kappa^{-1} = 44$ Å, decreases with smaller screening length, and has vanished at $\kappa^{-1} = 2.1$ Å. At $\kappa^{-1} = 44$ Å, the density outside the capsid is negligible, whereas at the two smaller values of κ^{-1} a significant density occurs. At $\kappa^{-1} = 7.0$ Å ($\kappa^{-1} \approx D_c$), the polyelectrolyte counterions are depleted from the outer capsid surface by the repulsive interaction with the positive net charge of the capsid, Z_c^{net} (see below). At the highest salt concentration $\kappa^{-1} = 2.1$ Å ($\kappa^{-1} \ll D_c$), the depletion is strongly

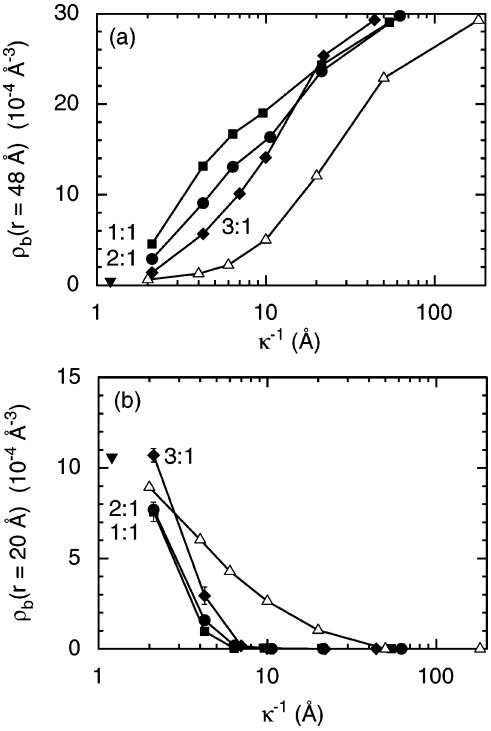

Figure 5. Bead number density $\rho_b(r)$ at the radial locations (a) $r = 48$ Å and (b) $r = 20$ Å as a function of the Debye screening length κ^{-1} using the primitive model in 1:1, 2:1, and 3:1 salt solutions (connected filled symbols) and the screened Coulomb model (open symbols) in a semilogarithmic representation. Bead number densities of the corresponding uncharged and encapsidated chain are also shown (nablas).

reduced owing to the increased electrostatic screening by the salt. Finally, the deficiency region next to the cell boundary originates from the absence of the polarizability beyond the cell border.[35,36]

The reduced density profiles of the capsid counterions are only weakly affected by the salt concentration unless the salt concentration is low (Figure 4c). At $\kappa^{-1} = 44$ Å, the probability of finding capsid counterions inside the capsid is very small. At further addition of salt, the presence of capsid counterions inside the capsid becomes significant, and the relative accumulation close to the capsid surfaces is reduced. Yet, the contact number density at the inner capsid surface remains sensibly large, about twice the average density at $\kappa^{-1} = 2.1$ Å, a distance which is half the contact distance between capsid counterions and capsid charges.

Figure 5 presents the bead number density for the 1:1, 2:1, and 3:1 salt solutions at the inner capsid surface ($r = 48$ Å) and at a radial distance inside the capsid ($r = 20$ Å) as a function of κ^{-1}. First, the general behavior of the reduction of the density at the inner capsid surface and the increase of the density closer to the center at increasing salt concentration has already been discussed. Furthermore, the bead densities at the inner capsid surface are independent of the valence of the polyelectrolyte counterions at high screening length, $\kappa^{-1} \geq 20$ Å, but at smaller screening lengths, the adsorption decreases with increasing cation valence at a given κ^{-1} (Figure 5a). At $r = 20$ Å, the bead densities are essentially zero for $\kappa^{-1} \geq 6$ Å, but at smaller screening lengths, nonzero densities are obtained, a higher density at larger cation valence (Figure 5b). Finally, at $\kappa^{-1} \approx 2$ Å with trivalent cations, the polyelectrolyte bead densities become essentially the same as for an uncharged polymer confined in an uncharged capsid (nabla). Obviously, the screening effect of the small ions is not fully captured by specifying the Debye screening length only. The discrepancy

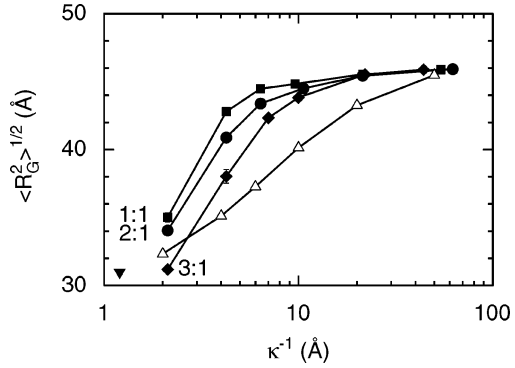

Figure 6. Radius of gyration of encapsidated polyelectrolyte $\langle R_G^2 \rangle^{1/2}$ as a function of the Debye screening length κ^{-1} using the primitive model in 1:1, 2:1, and 3:1 salt solutions (connected filled symbols) and the screened Coulomb model (open symbols) in a semilogarithmic representation. The radius of gyration of the corresponding uncharged and encapsidated chain is also shown (nabla).

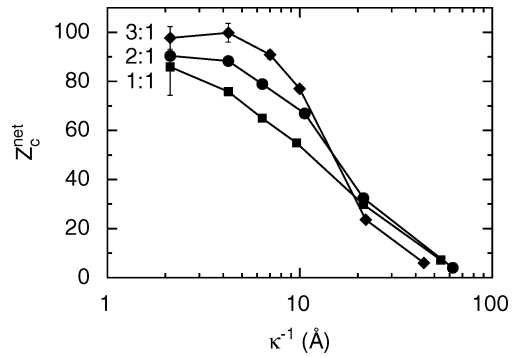

Figure 7. Capsid net charge Z_c^{net} as a function of the Debye screening length κ^{-1} in 1:1, 2:1, and 3:1 salt solutions in a semilogarithmic representation.

among the different solutions arises from the different importance of the spatial correlations. (In the mean-field Poisson−Bolztmann theory, the electrostatic screening arising from the small ions is independent of the small ion valences provided that κ^{-1} is the same for the solutions.)

To gain further insight into how the redistribution of beads toward the capsid center occurs at increasing salt concentration, Figure 6 displays the polyelectrolyte root-mean-square (rms) radius of gyration $\langle R_G^2 \rangle^{1/2}$ as a function of the Debye screening length κ^{-1} for the 1:1, 2:1, and 3:1 salt solutions. Irrespectively of the electrolyte type, at $\kappa^{-1} \geq 20$ Å (low salt concentration), we obtain $\langle R_G^2 \rangle^{1/2} \approx 45$ Å, implying the existence of a thin layer of beads adsorbed onto the inner capsid surface. At lower κ^{-1}, $\langle R_G^2 \rangle^{1/2}$ decreases with decreasing κ^{-1}, reflecting the redistribution of the beads from the surface to the center of the capsid (cf. Figure 4a). The effect sets in at lower salt concentration for higher polyelectrolyte counterion valence, in line with the valence dependence of the radial bead distribution. Finally, at $\kappa^{-1} = 2.0$ Å, in the case of the 3:1 salt solution, the value of $\langle R_G^2 \rangle^{1/2}$is the same as that of the equivalent neutral chain confined in an uncharged capsid of the same size (nabla).

Figure 7 shows the capsid net charge Z_c^{net}, given by the sum of all charged particles located at $r < R_c + D_c = 62$ Å, as a function of κ^{-1}. Independently of the salt concentration and of the polyelectrolyte counterion valence, the partition of the small ions is always such that $Z_c^{net} > 0$. Hence, the charge of the polyelectrolyte counterions exceeds that of the capsid counterions. The capsid net charge increases with (i) decreasing κ^{-1} (increasing salt concentration) and (ii) increasing polyelectrolyte counterion valence at fixed κ^{-1}. Noticeably, the increasing

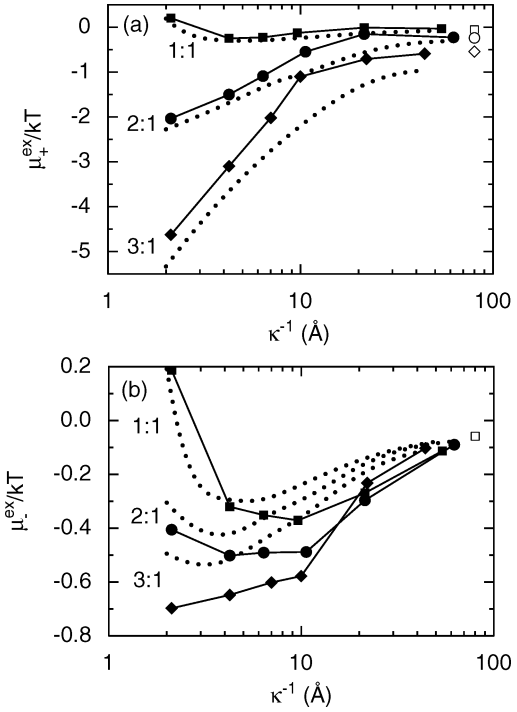

Figure 8. (a) Polyelectrolyte counterion and (b) capsid counterion reduced excess chemical potential μ_i^{ex}/kT as a function of the Debye screening length κ^{-1} in 1:1, 2:1, and 3:1 salt solutions for small ions residing outside the capsid (filled symbols) and in a pure salt solution (dotted curves) in a semilogarithmic representation. Data for the limiting case of salt-free polyelectrolyte-containing capsid are also given (open symbols).

excess of positive counterions inside the capsid levels off at $\kappa^{-1} \approx 4$ Å, where the net charge is ≈100e for the 3:1 salt solution.

Variation of Salt Concentration: Effects on the Excess Chemical Potential. As briefly discussed, the total absolute charge of the cations and that of the anions inside the capsid are not equal. The establishment of the Donnan equilibrium across the capsid was further investigated by calculating the excess chemical potentials of the individual salt species μ_i^{ex} inside and outside the capsid separately. It should be noted that the solution outside the capsid is not a bulk salt solution, since we have a nonzero capsid concentration through the finite cell size. The corresponding excess chemical potentials in bulk salt solutions $\mu_i^{ex,salt\ solution}$ obtained by using a cubic box with periodic boundary conditions applied will also be given.

Figure 8 shows the reduced excess chemical potential μ_i^{ex}/kT of the polyelectrolyte counterions (Figure 8a) and capsid counterions (Figure 8b) *outside* the capsid (filled symbols) and in a salt solution (dotted curves) at different screening lengths and polyelectrolyte counterion valences. We notice that (i) both cations and anions display a negative excess chemical potential in the capsid−salt solution and in the pure salt solution for the salt concentrations investigated except for the 1:1 solution at $\kappa^{-1} = 2.0$ Å and (ii) the magnitude of the excess chemical potential increases at decreasing κ^{-1} (increasing salt concentration) except for some cases at high salt concentration for the 1:1 and 2:1 solutions. It is interesting to compare the excess chemical potential for the solution outside the capsid with that for the corresponding salt solution, namely, $\Delta\mu_i^{ex} = \mu_i^{ex} - \mu_i^{ex,salt\ solution}$. Doing this, we find that (iii) the magnitude of the excess chemical potential of polyelectrolyte counterions is smaller in the polyelectrolyte-containing capsid system as compared with that in the salt solution ($\Delta\mu_+^{ex} > 0$), whereas the

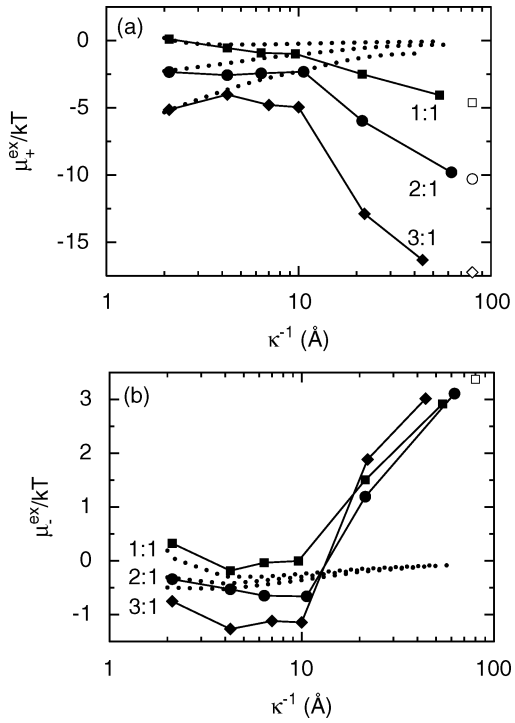

Figure 9. (a) Polyelectrolyte counterion and (b) capsid counterion reduced excess chemical potential μ_i^{ex}/kT as a function of the Debye screening length κ^{-1} in 1:1, 2:1, and 3:1 salt solutions for small ions residing inside the capsid (filled symbols) and in a pure salt solution (dotted curves) in a semilogarithmic representation. Data for the limiting case of salt-free polyelectrolyte-containing capsid are also given (open symbols).

opposite relation appears for the capsid counterions ($\Delta\mu_-^{ex} < 0$). Moreover, (iv) $\Delta\mu_+^{ex}$ and $\Delta\mu_-^{ex}$ display extreme values at $\kappa^{-1} \approx 10$ Å, and at the extreme point, $\Delta\mu_+^{ex}$ increases at increasing Z_+, whereas at the extreme point $\Delta\mu_-^{ex}$ is essentially independent of Z_+. For example, for $Z_+ = 3$, we have $\Delta\mu_+^{ex}/kT \approx +1$ at $\kappa^{-1} \approx 10$ Å. Finally, at the highest κ^{-1} ($\approx R_c$), the values of μ_i^{ex} are close to those of the corresponding salt-free case (open symbols).

Observations i and ii originate from the fact that the cohesiveness of the Coulomb interaction dominates over the hard-core repulsion for submolar salt concentrations,[33] and the hard-core repulsion becomes important only at high salt concentrations. Regarding observation iii, it can be rationalized by the fact that the capsid net charge Z_c^{net} is positive at all concentrations. Thus, it is energetically more favorable to add a capsid counterion instead of a polyelectrolyte counterion to the solution outside the capsid. The last issue, the non-monotonic behavior of $\Delta\mu_i^{ex}$ at increasing salt concentration, can be understood by considering two competing aspects: an increase of Z_c^{net} at reduced κ^{-1} (Figure 7) leading to an enhancement of $|\Delta\mu_i^{ex}|$ and an increased electrostatic screening reducing the effect of Z_c^{net} on $|\Delta\mu_i^{ex}|$. Obviously, the first dependence dominates at low screening, and the second one dominates at high screening.

The reduced excess chemical potential of polyelectrolyte and capsid counterions *inside* the capsid (filled symbols) as well as the corresponding values in the salt solution (dotted curves) are shown in Figure 9. First, at low salt concentration, μ_i^{ex} for the small ions deviates strongly from $\mu_i^{ex,salt\ solution}$, in contrary to the behavior outside the capsid. In more detail, $\Delta\mu_+^{ex}/kT \ll 0$ and $\Delta\mu_-^{ex}/kT \gg 0$ at low and moderate salt concentrations; hence, the conditions differ markedly from those in a salt

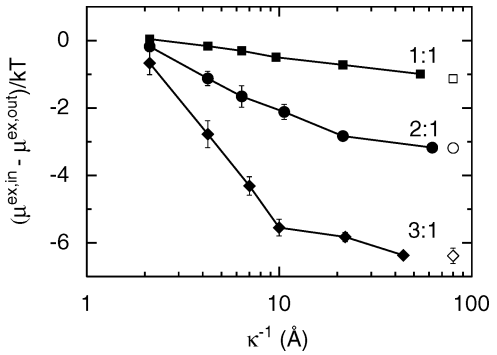

Figure 10. Difference in the reduced excess chemical potential of the simple salt between the capsid interior and the capsid exterior as a function of κ^{-1} in 1:1, 2:1, and 3:1 salt solutions (filled symbols) in a semilegarithmic representation. (These data are consistent with the densities of the small ions inside and outside the capsid through $\mu = kT\rho_+^{\nu}+ \rho_-^{\nu}- + \mu^{ex}$ applied separately to the solution inside and outside the capsid and $\mu^{in} = \mu^{out}$.) Data for the limiting case of salt-free polyelectrolyte-containing capsid are also given (open symbols).

solution. Moreover, the magnitude of $\Delta\mu_+^{ex}$ increases with increasing Z_+. Again, at $\kappa^{-1} \approx R_c$, the values of μ_i^{ex} are close to those of the corresponding salt-free case (open symbols). These observations imply a strong preference for the cations over the anions to be inside the capsid, which originates from the presence of the negatively charged polyelectrolyte. Second, at increasing salt concentration, and similar to the case outside of the capsid, μ_i^{ex} for the small ions approaches $\mu_i^{ex,salt\ solution}$, and the effect of hard-core repulsion on the excess chemical potential becomes significant in the case of anions at the highest salt content.

The difference between the reduced excess chemical potential of the simple salt (see eq 14) inside the capsid and that outside the capsid, $(\mu^{ex,in} - \mu^{ex,out})/kT$, representing the Donnan potential established between the two regions in kT units,[37] is displayed in Figure 10 as a function of the Debye screening length κ^{-1}. Owing to the presence of the encapsidated polyelectrolyte, the chemical potential of the simple salt inside the capsid is more negative than that outside the capsid. At $\kappa^{-1} \approx 50$ Å, the difference has essentially approached that of the corresponding salt-free system and amounts to $-1kT$ for the 1:1 salt solution and to about $-6kT$ for the 3:1 salt solution. As expected, when the electrostatic interaction is screened at lower κ^{-1}, the difference between the excess chemical potential inside the capsid and that outside the capsid decreases. At $\kappa^{-1} = 2.1$ Å, $(\mu^{ex,in} - \mu^{ex,out})/kT$ is close to zero and hardly depends on Z_+ any more.

Screened Coulomb Model. As mentioned in the model section, the structure of an encapsidated polyelectrolyte has also been examined with a screened Coulomb model. Instead of being explicitly included in the system, the small ions now screen the remaining Coulomb interactions in the system through a screened Coulomb potential (eqs 5 and 6). Such a coarse-grained description works best when the small ions are homogeneously distributed. Hence, it is not obvious that such an approach is appropriate in the present case.

In addition to the bead number density at the inner capsid surface and at $r = 20$ Å using the primitive model (filled symbols), Figure 5 also displays the same property using the screened Coulomb model (open symbols). Qualitatively, the latter model also predicts an increase of the bead number density in the central region of the capsid (Figure 5b) at the expense of the beads density near the inner capsid surface (Figure 5a) at increasing salt concentration. Nonetheless, the bead number

density at the inner capsid surface is systematically underestimated. Under physiological salt conditions, $\kappa^{-1} \approx 10$ Å, the number density is underestimated by approximately three times as compared with the primitive model. Consequently, the Coulomb model overestimates the bead density in the capsid center. At $\kappa^{-1} \approx 10$ Å, a significant bead density is predicted, whereas a practically zero density is obtained from the primitive model.

Figure 6 also includes the rms radius of gyration $\langle R_G^2 \rangle^{1/2}$ as a function of the Debye screening length κ^{-1} using the screened Coulomb model (open symbols). Consistently with the radial bead distribution, the screened Coulomb model predicts a qualitatively correct result; that is, $\langle R_G^2 \rangle^{1/2} = 45$ Å at low salt concentration and a contraction of the polyelectrolyte appears at increasing salt concentration. However, the contraction starts at a higher κ^{-1} (lower salt concentration), leading to an underestimate of the radius of gyration at $\kappa^{-1} < 40$ Å. The approach to the result of the primitive model at high salt concentration appears in the regime where the electrostatic interaction is essentially fully screened.

Thus, the adsorption of the polyelectrolyte at the inner capsid surface is electrostatically driven. Since the adsorption is weaker in the screened Coulomb approach, we conclude that the electrostatic screening predicted by the screened Coulomb model is exaggerated. We suggest that a significant contribution to the exaggerated screening occurring in the Coulomb model arises from the formal access for the small ions to the volume occupied by the shell, as impled by eq 6.

Conclusions

Monte Carlo simulations have been employed to determine properties of a model system representing a flexible polyelectrolyte confined inside an oppositely charged capsid at different concentration of simple salt and salt valence. The electrostatic interaction has been handled using two different approaches: the primitive model and the screened Coulomb model.

The main findings and conclusions are as follows:

(A) The valence of the polyelectrolyte counterions affects (i) the radial profiles of all charged species, (ii) the net charge of the capsid, (iii) the excess chemical potential of the small ions inside the capsid, and (iv) the Donnan equilibrium established between the inner and the outer regions.

(B) At low salt content ($\kappa^{-1} > 50$ Å), the polyelectrolyte is found exclusively as a single layer near the inner capsid surface, and at increasing salt content, a broader radial distribution is obtained. When $\kappa^{-1} \approx 5$ Å, the central void is strongly reduced, and at higher salt concentration, the polyelectrolyte occupies the full capsid interior but with a depletion layer at the inner capsid surface. The adsorption of the polyelectrolyte at low salt content is a combination of a replacement of adsorbed capsid counterions with adsorbed beads and a reduction of the electrostatic bead−bead repulsion.

(C) The net charge of the capsid Z_c^{net} is of the same sign as the charge of the capsid and increases with increasing salt concentration. Consequently, a model with an explicit representation of the salt species is necessary for a qualitatively correct prediction of the net charge of viruses.

(D) The amplitude of the excess chemical potential of the small ions inside a polyelectrolyte-containing capsid is very different as compared with a simple salt solution. The difference is dependent on the valence of the polyelectrolyte counterion, and it diminishes progressively at increasing salt content.

(E) The simplified screened Coulomb model of the extended Debye−Hückel type exaggerates the electrostatic screening and predicts a too weak adsorption of the polyelectrolyte at the inner capsid surface. At physiological salt conditions, the salt concentration has to be reduced 10 fold to give the similar structure as that predicted by the primitive model.

The present study is based on a model representing scaled-down RNA-containing viruses. Nevertheless, the effect of the electrostatic interaction and the screening of the salt are of such general character that the present observations are operating in real virus systems. Some of our findings could possibly be tested by electron microscopy, neutron scattering, and electrophoretic mobility. After a basic understanding of the electrostatic interactions, it would be interesting to extend the model by refining the description of the capsid by including titratable charges, nonspherical shapes, and hydrophobic interactions as well as increasing the size of the model system.

Acknowledgment. Financial support from the Swedish Research Council (VR) is gratefully acknowledged.

References and Notes

(1) Brenner, D.; Lyshefski, S.; Iafrate, G.; Goddard, W. A., III, *Handbook of nanoscience engineering and technology*; CRC Press, Boca Raton, FL, 2002.
(2) Bancroft, J. B. *Adv. Virus Res.* **1970**, *16*, 99.
(3) Klug, A. C. H.; Finch, J. T.; Klug, A. *Nature (London)* **1971**, *229*, 37.
(4) Ceres, P.; Zlotnick, A. *Biochemistry* **2002**, *41*, 11525.
(5) Schoot, P. v. d.; Bruinsma, R. *Phys. Rev. E* **2005**, *71*, 061928.
(6) Bink, H. H.; Pleij, C. W. *Arch. Virol.* **2002**, *147*, 2261.
(7) Tsuruta, H.; Reddy, V. S.; Wikoff, W. R.; Johnson, J. E. *J. Mol. Biol.* **1998**, *284*, 1998.
(8) Jardine, P. J.; Anderson, D. L. DNA packaging in the bacteriophages. In *The Bacteriophages*; Oxford University Press: New York, 2006.
(9) Purohit, P. K.; Inamdar, M. M.; Grayson, P. D.; Squires, T. M.; Kondev, J. *Biophys. J.* **2005**, *88*, 851.
(10) Kindt, J.; Tzlil, S.; Ben-Shaul, A.; Gelbart, W. M. *Proc. Natl. Acad. Sci.* **2001**, *98*, 13671.
(11) Purohit, P. K.; Kondev, J.; Phillips, R. *Proc. Natl. Acad. Sci.* **2003**, *100*, 3173.
(12) Earnshaw, W. C.; Harisson, S. C. *Nature* **1977**, *268*, 598.
(13) Beer, S. V.; Kosuge, T. *Virology* **1970**, *40*, 930.
(14) Jonard, G.; Witz, J.; Hirth, L. *J. Mol. Biol.* **1972**, *67*, 165.
(15) Evilevitch, A.; Castelnovo, M.; Knobler, C. M.; Gelbart, W. M. *J. Phys. Chem. B* **2004**, *108*, 6838.
(16) Castelnovo, M.; Evilevitch, A. *Europhys. Lett.* **2006**, *73*, 635.
(17) Arsuaga, J.; Tan, R. K.-Z.; Vasquez, M.; Sumners, D.; Harvey, S. C. *Biophys. Chem.* **2002**, *101−102*, 475.
(18) Marenduzzo, D.; Micheletti, C. *J. Mol. Biol.* **2003**, *330*, 485.
(19) LaMarque, J. C.; Le, T. L.; Harvey, S. C. *Biopolymers* **2004**, *73*, 348.
(20) Spakowitz, A. J.; Wang, Z.-G. *Biophys. J.* **2005**, *88*, 3912.
(21) Forrey, C.; Muthukumar, M. *Biophys. J.* **2006**, *91*, 25.
(22) Angelescu, D. G.; Bruinsma, R.; Linse, P. *Phys. Rev. E* **2006**, *73*, 041921.
(23) Angelescu, D.; Linse, P. *Phys. Rev. E* **2007**, in press.
(24) Freddolino, P. L.; Arkhipov, A. S.; Larson, S. B.; McPherson, A.; Schulten, K. *Structure* **2006**, *14*, 437.
(25) Cerritelli, M. E.; Cheng, N.; Rosenberg, A. H.; McPherson, C. E.; Booy, F. P.; Steven, A. C. *Cell* **1997**, *91*, 271.
(26) Fokine, A.; Chipman, P. R.; Leiman, P. G.; Mesyanzhinov, V. V.; Rao, V. B.; Rossmann, M. G. *Proc. Natl. Acad. Sci.* **2004**, *101*, 6003.
(27) Zhang, D.; Konecny, R.; Baker, N. A.; McCammon, J. A. *Biopolymers* **2004**, *75*, 323.
(28) Stukan, M. R.; Lobaskin, V.; Holm, C.; Vinogradova, O. *Phys. Rev. E* **2006**, *73*, 021801.
(29) Akinchina, A.; Linse, P. *Macromolecules* **2002**, *35*, 5183.
(30) Linse, P. *MOLSIM 4.0.7 version*; Lund University: Lund, Sweden, 2005.
(31) Widom, B. *J. Chem. Phys.* **1963**, *39*, 2808.
(32) Svensson, R. R.; Woodward, C. E. *Mol. Phys.* **1988**, *64*, 247.
(33) Edgecombe, S.; Schneider, S.; Linse, P. *Macromolecules* **2004**, *26*, 10089.
(34) Pais, A. A. C. C.; Miguel, M. G.; Linse, P.; Lindman, B. *J. Chem. Phys.* **2002**, *117*, 1385.
(35) Wennerström, H.; Jönsson, B.; Linse, P. *J. Chem. Phys.* **1982**, *76*, 4665.
(36) Netz, R. R.; Joanny, J. F. *Macromolecules* **1999**, *32*, 9013.
(37) Mafé, S.; Manzanares, J. A.; Reiss, H. *J. Chem. Phys.* **1993**, *98*, 2325.